Electronic Supplementary Information

Oxygen vacancy enriched $Na_{1.19}V_8O_{20}$ $4.42H_2O$ nanosheets for fast and stable Zn-ion battery

Mengcheng Wu,[a] Jie Li, [a] Mengda Xue,[a] Xun Zhao,[a] Lei Mao,[a] and Lingyun Chen *[a]

[a] School of Chemistry and Chemical Engineering, Chongqing University, Chongqing 400044, P. R. China

*E-mail: lychen@cqu.edu.cn (L. Chen)

Experimental section

1. Materials preparation

1.1 Synthesis of $VOPO_4$ $2H_2O$

Firstly, 2.4 g of V_2O_5 powder was added into 57.7 mL of deionized water following by magnetic stirring for 10 minutes. Then, 13.3 mL of concentrated H_3PO_4 was added into the above solution and magnetically stirred for 2.0 h. Subsequently, the mixed solution was transferred into a 100 mL Teflon-lined stainless-steel autoclave and heated to 120 °C for 16 h. Finally, the obtained yellow product was washed with water and acetone three times, respectively, and then dried at 60°C for 12 h under vacuum.

1.2. Synthesis of V_o-NVO-2

V_o-NVO-2 are prepared through a facile one-step hydrothermal method. Briefly, 200 mg of as-prepared $VOPO_4$ $2H_2O$ and 25.2 mg of Na_2SO_3 were dispersed in 60 mL of deionized water and magnetically stirred for 20 minutes. Afterwards, the mixed solution was transferred into a 100 mL Teflon-lined stainless-steel autoclave and heated to 180 ° C for 16 hours. Finally, the V_o-NVO-2 sample was collected through filtration and washed three times with water and ethanol respectively. The sample was dried in a vacuum oven at 80 °C for 12 h. NVO and V_o-NVO-2 were prepared using the same process, except that 0.2 mmol Na_2SO_3 was replaced with 0.2 mmol Na_2SO_4 and a mixture of 0.1 mmol Na_2SO_3 and 0.1 mmol Na_2SO_4, respectively.

2. Materials characterization

The X-ray diffraction (XRD) patterns were performed using the Bruker D8 Advance powder diffractometer with a Cu Kα radiation (λ =1.5406 Å) to determine their crystal structure information of the samples. Inductively coupled plasma optical emission spectrometer (ICP-OES, Agilent 5110) was used to analyze the element ratios. Thermogravimetric analysis (TGA, Mettler Toledo TGA2)

was carried out to detect the content of structural water. The microstructure of the samples was observed through scanning electron microscopy (SEM, Quattro S). Transmission electron microscope (TEM) images, selected area electron diffraction (SAED), energy dispersive spectrometry (EDS) spectra and element mapping were obtained using transmission electron microscope (Talos F200S). X-ray photoelectron spectroscopy (XPS) was conducted on the Thermo Scientific K-Alpha electron spectrometer. The oxygen vacancies in the samples were characterized by electron paramagnetic resonance (EPR) (Bruker EMXplus). Raman spectra was performed by laser confocal Raman spectrometer (Raman, LabRAM HR Evolution) under laser excitation at 532 nm.

3. Electrochemical measurement

For the preparation of cathode, polyvinylidene fluoride, acetylene black, and active materials were fully mixed in N-methyl-2-pyrrolidone solvent with a mass ratio of 1:2:7 and then the slurry was uniformly coated on titanium foil and dried at 80°C for 12 h under vacuum. The mass loading of the active materials was 1.2~1.6 mg cm^{-2}. The aqueous ZIBs were assembled with zinc foil as the anode, glass fiber membrane as the separator, and 2 M $Zn(CF_3SO_3)_2$ aqueous solution as the electrolyte. Galvanostatic charge/discharge (GCD) and galvanostatic intermittent titration technique (GITT) tests were conducted via a LAND battery testing system (CT3001A) within the voltage window of 0.2−1.6 V. Cyclic voltammogram (CV) and electrochemical impedance spectroscopy (EIS) were performed with a CHI660E electrochemical workstation.

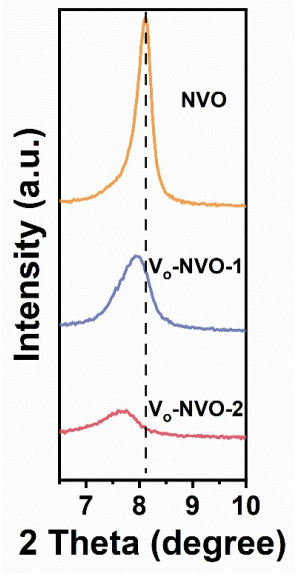

Fig. S1. The partial enlarged XRD pattern.

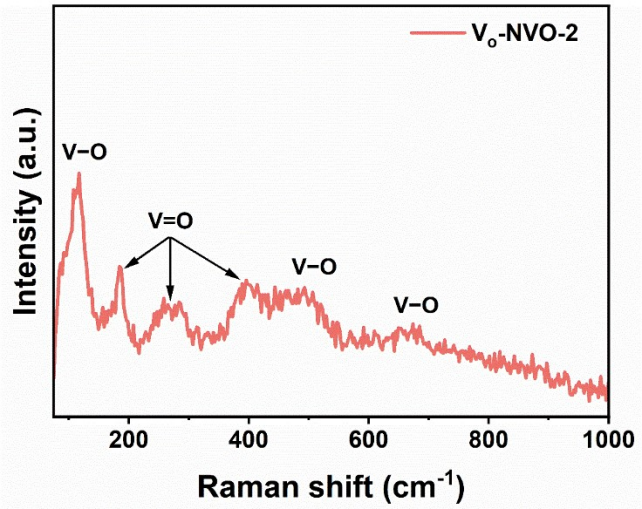

Fig. S2. The Raman spectrum of V_o-NVO-2 sample.

The peaks of V_o-NVO-2 located at 116, 484, and 684 cm^{-1} could be attributed to bending and stretching vibration mode of V−O bonds, while the bending vibration of V=O bonds can be detected at the peaks of 188, 264, and 402 cm^{-1}.[1, 2]

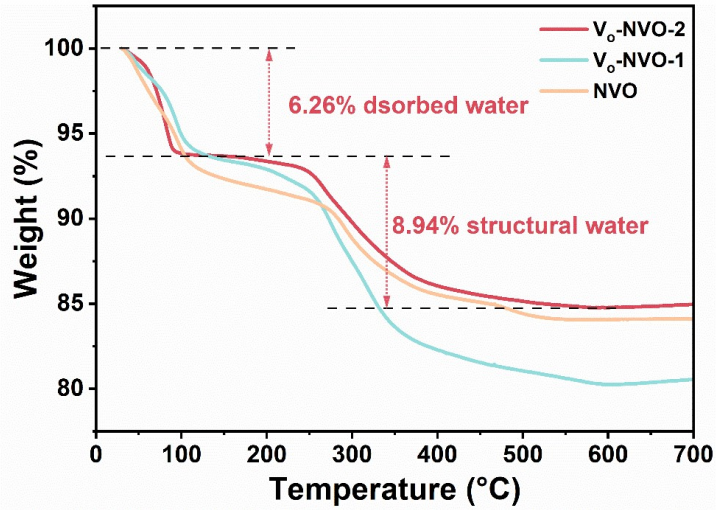

Fig. S3. The TGA curves V_o-NVO-2, V_o-NVO-1, and NVO.

The TGA curves in Fig. S3 show that V_o-NVO-2, V_o-NVO-1, and NVO all have rich structural water content, which are 8.94%, 12.99%, and 7.54%, respectively. An appropriate amount of structural water can boost ion transport by shielding the effective charge of Zn^{2+} ions while reducing the hindrance to the migration of Zn^{2+} ions, enabling fast Zn^{2+} storage.[3] However, it cannot be ignored that the structural water accompanied by abundant hydrogen bonding will cause channel blockage, which hinders ion migration.[4] Thererfore, excessive structural water is detrimental to the performance of materials.

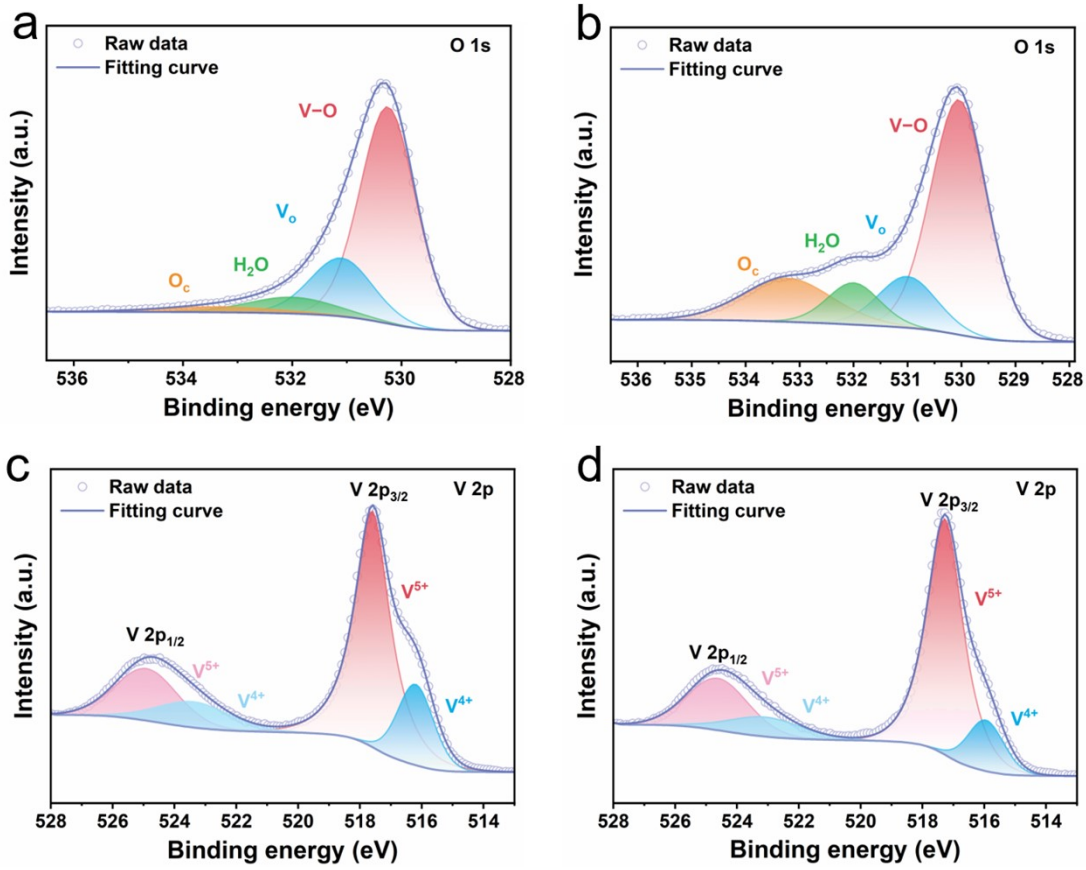

Fig. S4. The O 1s fine spectra of (a) V_o-NVO-1 and (b) NVO. The V 2p fine spectra of (c) V_o-NVO-1 and (d) NVO.

According to the peak area ratio of V $2p_{3/2}$ with different vanadium valence states in the V 2p XPS spectra,[5] the average valence state of vanadium on the material surface can be calculated using the following formula:

$$V_a = 5 \times \frac{m}{m+n} + 4 \times \frac{n}{m+n}$$

Where V_a represents the average valence state of vanadium, m is the peak area of V^{5+} in V $2p_{3/2}$ characteristic peak, and n is the peak area of V^{4+} in V $2p_{3/2}$ characteristic peak.

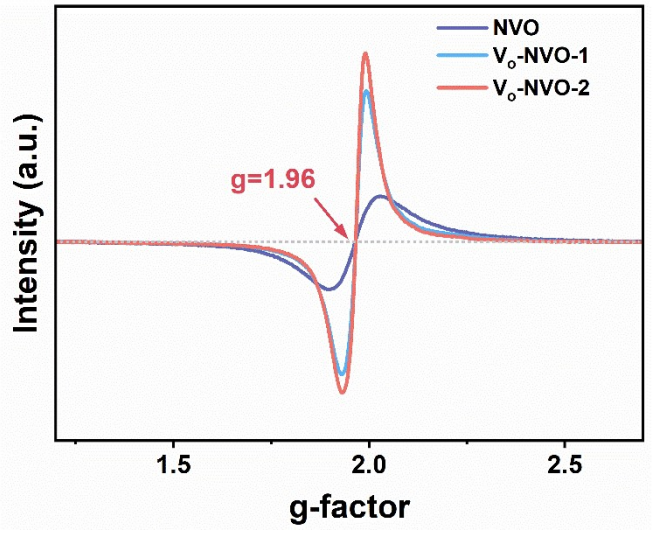

Fig. S5. The EPR spectra of V_o-NVO-2, V_o-NVO-1, and NVO.

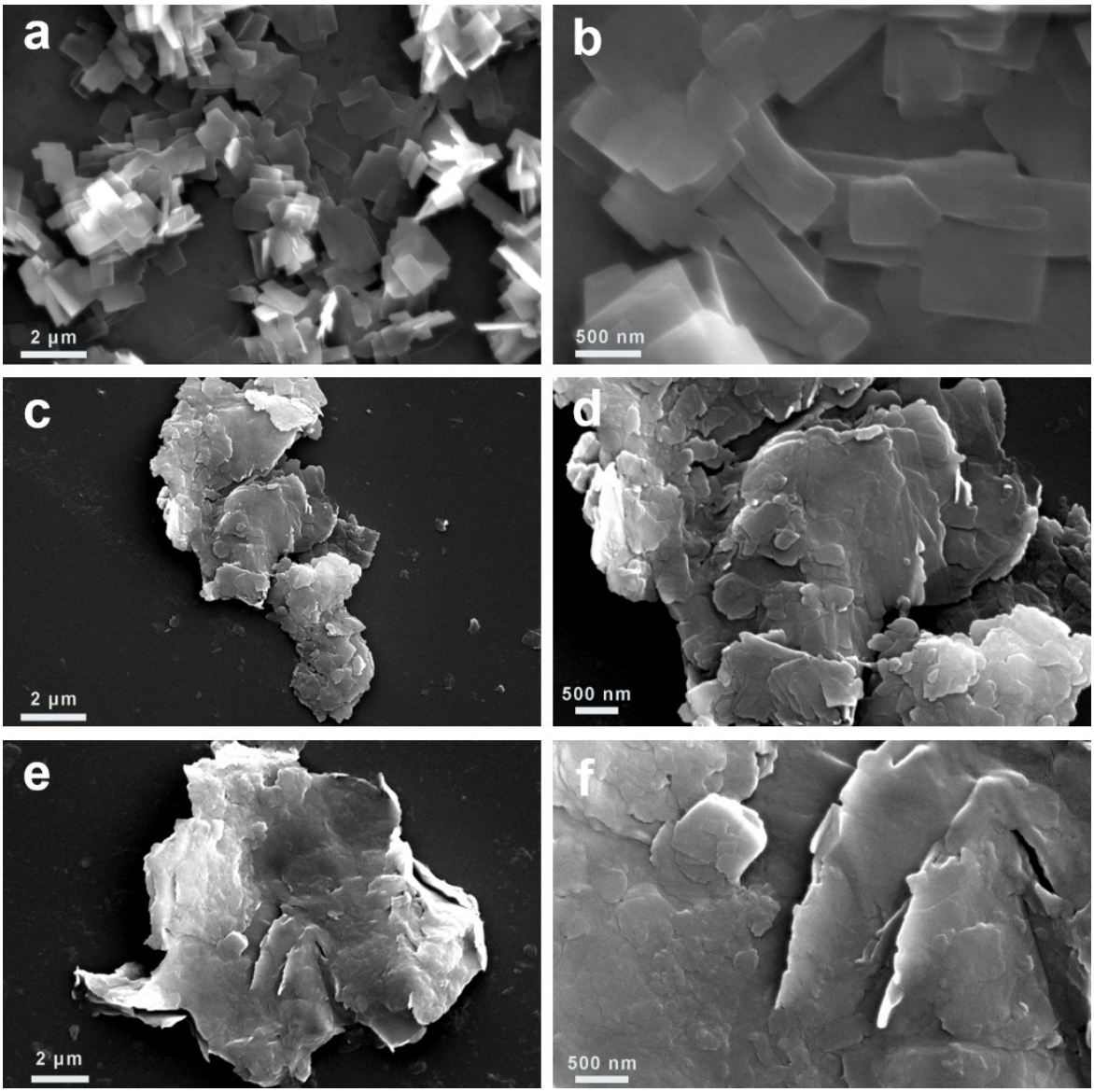

Fig. S6. The SEM images of (a-b) V_o-NVO-2, (c-d) V_o-NVO-1, and (e-f) NVO.

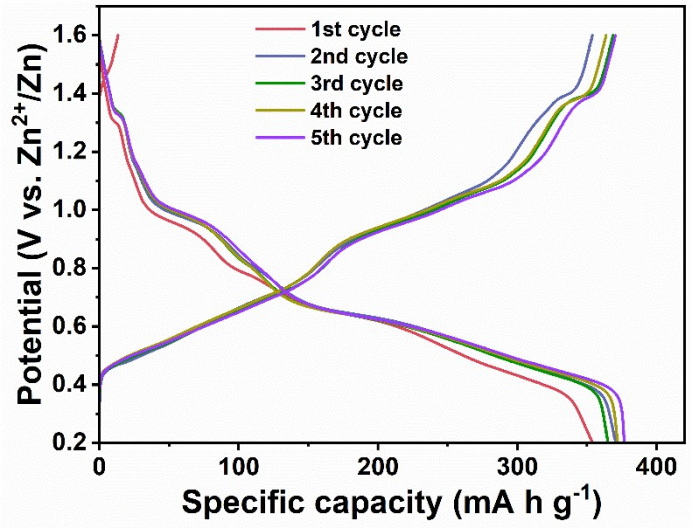

Fig. S7. The GCD curves of V_o-NVO-2 at the 0.1 A g^{-1}.

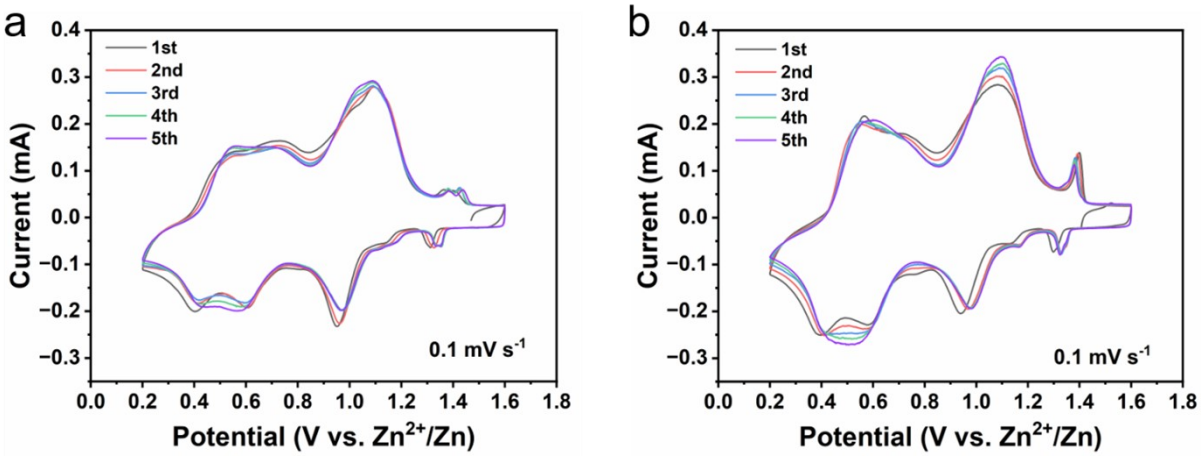

Fig. S8. The CV curves of (a) NVO and (b) V_o-NVO-1 at the scan rate of 0.1 mV s^{-1}.

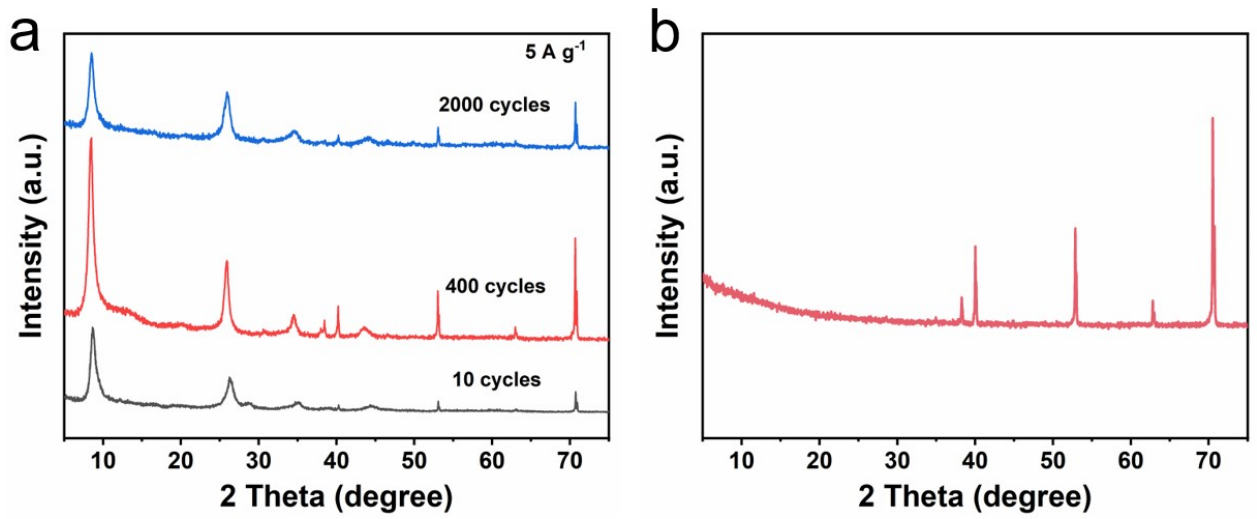

Fig. S9. (a) Ex-situ XRD patterns of V_o-NVO-2 at the 10th cycle, 400th cycle and 2000th cycle. (b) XRD pattern of titanium foil.

Based on the XRD images of V_o-NVO-2 after different cycles at 5 A g^{-1}, it is found that the interlayer spacing expands with the number of cycles increasing from 10 to 400, which may be due to the gradually trapped Zn^{2+} in the irreversible sites widens the interlayer spacing. Then the interlayer spacing hardly changes during the subsequent cycle to 2000 cycles, indicating that the V_o-NVO-2 has basically reached a stable charging/discharging state after 400 cycles.

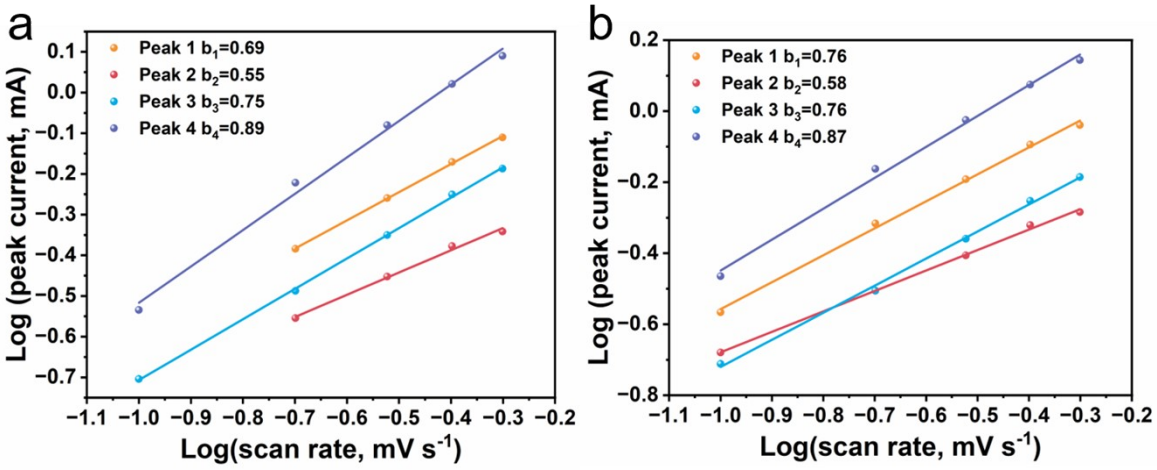

Fig. S10. The fitting b values of (a) NVO and (b) V_o-NVO-1.

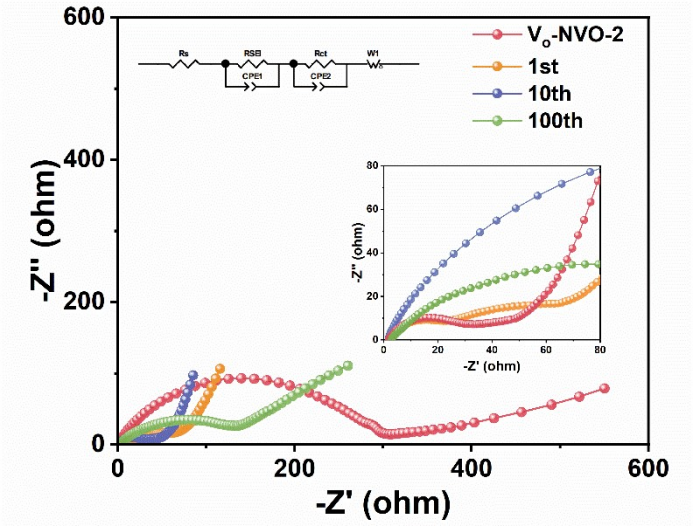

Fig. S11. EIS curves of V_o-NVO-2 at pristine state, after 1 cycle, after 10 cycles, and after 100 cycles at 0.1 A g^{-1}.

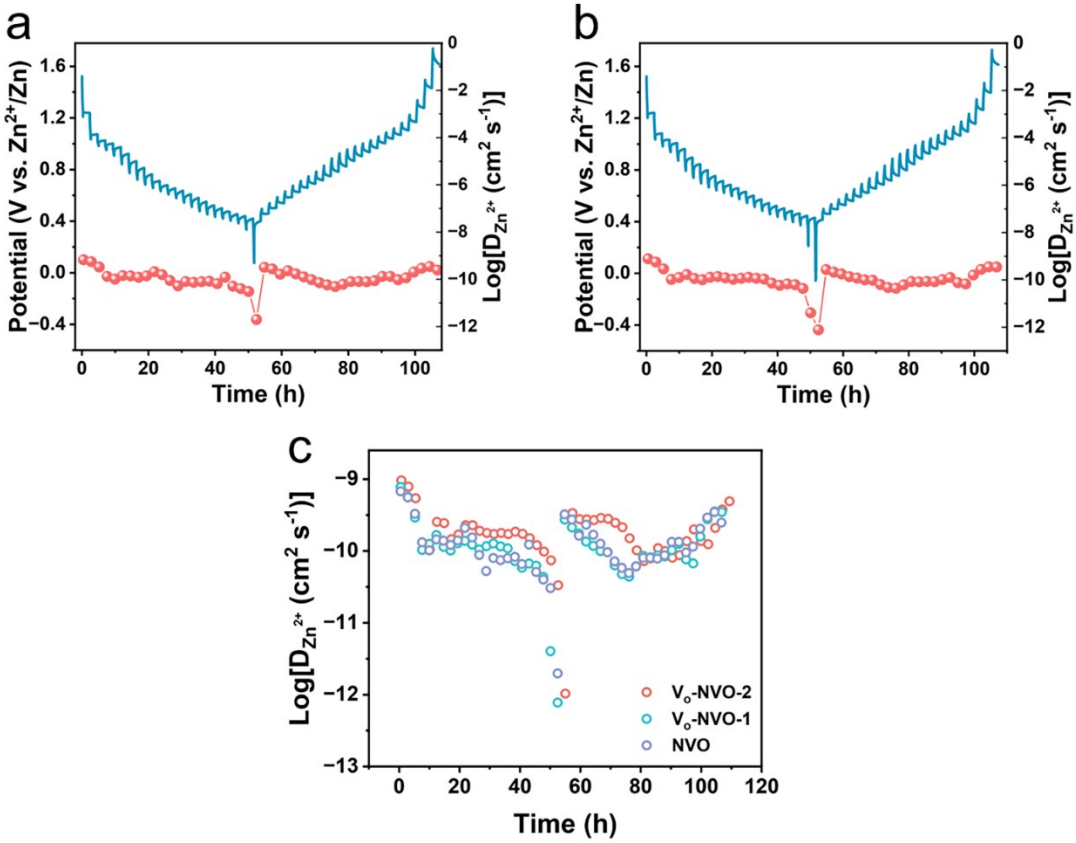

Fig. S12. The GITT curve and corresponding Zn^{2+} diffusion coefficient of (a) NVO and (b) V_o-NVO-1, (c) the comparsion Zn^{2+} diffusion coefficient of V_o-NVO-2, V_o-NVO-1, and NVO.

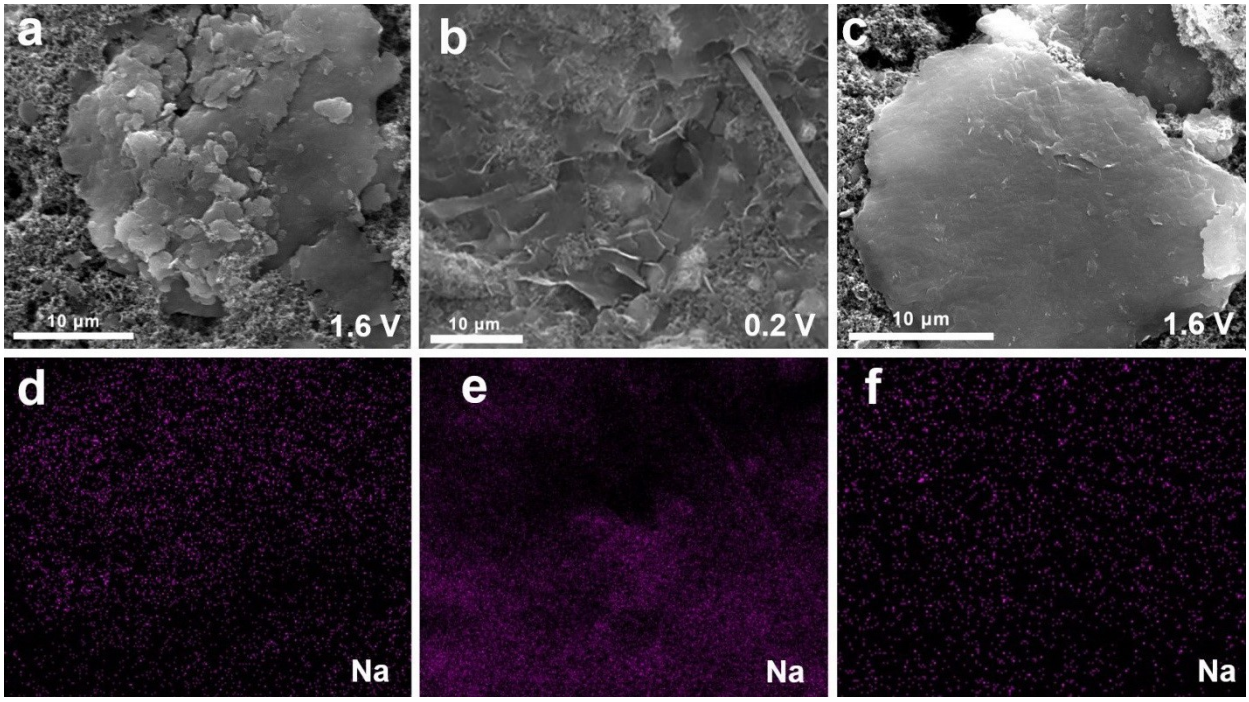

Fig. S13. The SEM images and element mapping images of the V_o-NVO-2 electrode in the (a, d) 1.6 V and (b, e) 0.2 V, (c, f) 1.6 V.

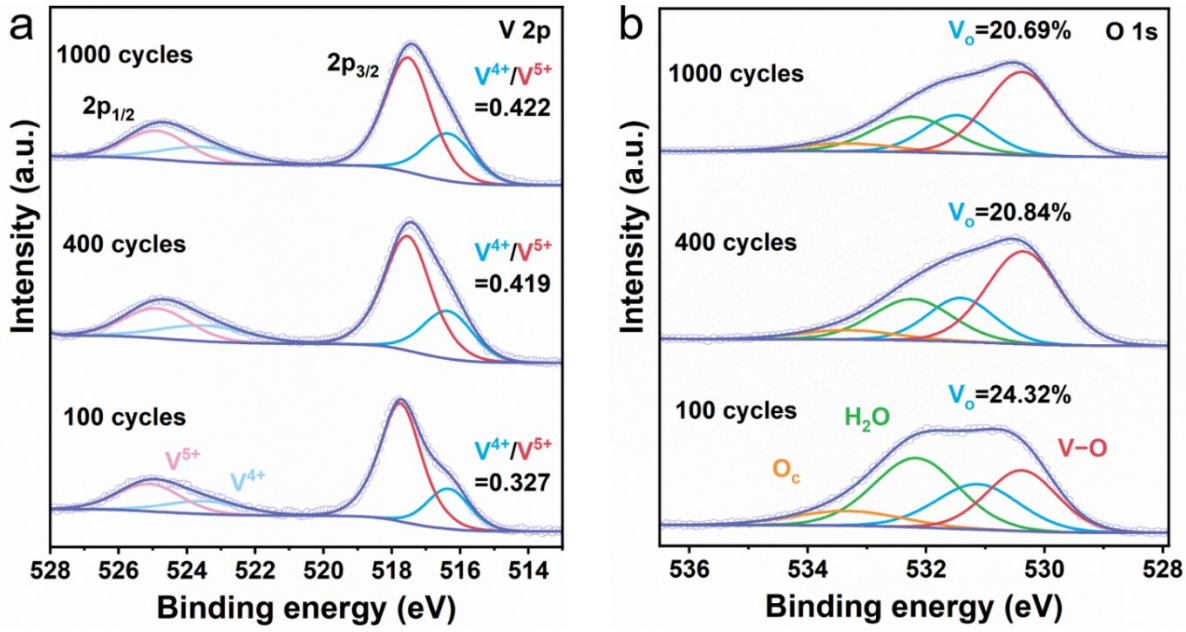

Fig. S14. The XPS spectra of (a) V 2p and (b) O 1s of V_o-NVO-2 after 100 cycles, 400 cycles, and 1000 cycles at 5 A g^{-1}.

The XPS fine spectra of V 2p and O 1s measured after different cycles of V_o-NVO-2 at 5A g^{-1} are shown in Fig. S14. We found that as the number of cycles increases, the proportion of V^{4+} in V_o-NVO-2 gradually increases, indicating a decrease in the average valence state of vanadium. After 400 cycles, the ratio of V^{4+}/V^{5+} is 0.419, corresponding to an average valence state of 4.70 for vanadium. This phenomenon suggests that the active sites in V_o-NVO-2 are gradually occupied by Zn^{2+} during the cycling process, leading to a continuous decrease in the valence state of vanadium. It is worth noting that after 400 cycles, the valence state of vanadium in V_o-NVO-2 hardly changes, indicating the material has reached a relatively stable state. The variation of oxygen vacancy content in the O 1s spectrum shows a same trend with vanadium valence state. These phenomena confirm the high stability and reversibility of materials during long-term cycling.

Table S1 The ICP-OES result of the V_o-NVO-2

Element	Mass content (%)	Molar ratio
Na	3.39	1.19
V	50.53	8.0

Table S2 Comparison of the resistance values of NVO, V_o-NVO-1, V_o-NVO-2.

State	R_s (Ω)	R_{ct} (Ω)
NVO	1.65	689.6
V_o-NVO-1	1.26	421.7
V_o-NVO-2	1.352	275.6

Table S3 Comparison of the resistance values of V_o-NVO-2 measured at pristine, after 1cycle, 10 cycles, and 100 cycles.

State	R_s (Ω)	R_{SEI} (Ω)	R_{ct} (Ω)
Pristine	1.352	-	275.6
1th cycle	2.07	16.63	59.47
10th cycle	1.698	26.07	9.022
100th cycle	2.577	28.5	91.83

Supplementary references

1 X. Wang, Y. Wang, A. Naveed, G. Li, H. Zhang, Y. Zhou, A. Dou, M. Su, Y. Liu, R. Guo and C. C. Li, *Adv. Funct. Mater.*, 2023, 2306205.

2 S. Zhang, Z. Zou, Y. Gao, J. Geng, M. Chen, W. Ling, F. Liang, X. Peng, M. Zhou, F. Yu and S. Jia, *Nano Energy*, 2023, **115**, 108736.

3 H. He, F.-C. Pan, X.-W. Liang, Q. Hu, S. Liu, J. Hu, S. C. Jun, D. Lin, Y. Yamauchi and Y. Huo, *Chem. Eng. J.*, 2023, **462**, 142221.

4 K. Yang, Y. Hu, L. Li, L. Cui, L. He, S. Wang, J. Zhao and Y.-F. Song, *Nano Energy*, 2020, **74**, 104851.

5 M. Du, C. Liu, F. Zhang, W. Dong, X. Zhang, Y. Sang, J.-J. Wang, Y.-G. Guo, H. Liu and S. Wang, *Advanced Science*, 2020, **7**, 2000083.